

Enhancing photovoltaic output power by 3-band spectrum-splitting and concentration using a diffractive micro-optic

Nabil Mohammad,¹ Peng Wang,¹ Daniel J. Friedman² and Rajesh Menon^{1,*}

¹Department of Electrical & Computer Engineering, University of Utah, Salt Lake City, UT 84112 USA

²National Renewable Energy Laboratory, Golden, CO 80401 USA

*rmemon@eng.utah.edu

Abstract: We report the enhancement of photovoltaic output power by separating the incident spectrum into 3 bands, and concentrating these bands onto 3 different photovoltaic cells. The spectrum-splitting and concentration is achieved via a thin, planar micro-optical element that demonstrates high optical efficiency over the entire spectrum of interest. The optic (which we call a polychromat) was designed using a modified version of the direct-binary-search algorithm. The polychromat was fabricated using grayscale lithography. Rigorous optical characterization demonstrates excellent agreement with simulation results. Electrical characterization of the solar cells made from GaInP, GaAs and Si indicate increase in the peak output power density of 43.63%, 30.84% and 30.86%, respectively when compared to normal operation without the polychromat. This represents an overall increase of 35.52% in output power density. The potential for cost-effective large-area manufacturing and for high system efficiencies makes our approach a strong candidate for low cost solar power.

©2014 Optical Society of America

OCIS codes: (350.6050) Solar energy; (050.1970) Diffractive optics; (230.3990) Micro-optical devices.

References and links

1. A. Polman and H. A. Atwater, "Photonic design principles for ultrahigh-efficiency photovoltaics," *Nat. Mater.* **11**(3), 174–177 (2012).
2. A. G. Inenes and D. R. Mills, "Spectral beam splitting technology for increased conversion efficiency in solar concentrating systems: a review," *Sol. Energy Mater. Sol. Cells* **84**(1), 19–69 (2004).
3. A. Mojiri, R. Taylor, E. Thomsen, and G. Rosengarten, "Spectral beam splitting for efficient conversion of solar energy—A review," *Renew. Sustain. Energy Rev.* **28**, 654–663 (2013).
4. B. Mitchell, G. Peharz, G. Siefer, M. Peters, T. Gandy, J. C. Goldschmidt, J. Benick, S. W. Glunz, A. W. Bett, and F. Dimroth, "Four-junction spectral beam-splitting photovoltaic receiver with high optical efficiency," *Prog. Photovolt. Res. Appl.* **19**(1), 61–72 (2011).
5. R. K. Kostuk and G. Rosenberg, "Analysis and design of holographic solar concentrators," *Proc. SPIE* **7043**, 70430I (2008).
6. H. A. Macleod, *Thin-Film Optical Filters* (CRC Press, 2001).
7. G. Kim, J.-A. Domínguez-Caballero, and R. Menon, "Design and analysis of multi-wavelength diffractive optics," *Opt. Express* **20**(3), 2814–2823 (2012).
8. G. Kim, J.-A. Domínguez-Caballero, H. Lee, D. J. Friedman, and R. Menon, "Increased photovoltaic power output via diffractive spectrum separation," *Phys. Rev. Lett.* **110**(12), 123901 (2013).
9. P. Wang, J.-A. Domínguez-Caballero, D. Friedman, and R. Menon, "A new class of multi-bandgap high efficiency photovoltaics enabled by broadband diffractive optics," *Prog. Photovolt. Res. Appl.*, doi:10.1002/pip.2516.
10. M. S. Leite, R. L. Woo, J. N. Munday, W. D. Hong, S. Mesropian, D. C. Law, and H. A. Atwater, "Towards an optimized all lattice-matched InAlAs/InGaAsP/InGaAs multijunction solar cell with efficiency >50%," *Appl. Phys. Lett.* **102**(3), 033901 (2013).
11. L. Guo, "Recent progress in nanoimprint technology and its applications," *J. Phys. D Appl. Phys.* **37**(11), R123–R141 (2004).

1. Introduction

A single bandgap solar cell suffers from poor efficiency due to its inability to convert photons of all energy into charge carriers. This limitation results from two phenomena: non-absorption and thermalization [1]. In the former case photons having energy less than the bandgap are not absorbed at all, while those having higher energy than the bandgap lose the excess energy by dissipating heat rapidly within the semiconductor. This limitation can be overcome by utilizing solar cells with different bandgaps and illuminating them with appropriate spectral bands. This demands an efficient method of spectrum splitting. Various spectrum-splitting strategies have been proposed in literature. A detailed review on spectrum-splitting methods for solar applications has been presented in [2]. Recent advances in spectrum-splitting based efficiency improvement in photovoltaics have been discussed in [3].

Spectrum splitting techniques are usually based on refraction, interference or diffraction. One simple example of refraction-based splitting is the use of a prism [2]. A prism refracts the incident light into several bands. This spectrally dispersed light can then be directed onto absorbers with matching band-gaps. Dichroic mirrors [4] and conventional gratings facilitate spectrum splitting via interference and diffraction, respectively. Other examples of spectrum splitting are the use of a holographic solar concentrator [5] and thin-film interference filters [2,6]. Holographic solar concentrators can choose the useful bands of incident sunlight selectively and concentrate them simultaneously. In interference optical filters multiple thin layers of dielectric materials with high refractive index contrast are deposited on a transparent substrate to achieve the properties of band-stop, band pass or edge filters [2,6]. Although these approaches offer spectrum splitting and have potential to be incorporated into photovoltaic systems, they suffer from multiple drawbacks. One major disadvantage is the associated increase in cost. Other drawbacks are the inability to scale to large areas, low wavelength-averaged optical efficiencies, and poor control of the position, number and size of the spectral bands.

To overcome these limitations, we introduced broadband diffractive optics for spectrum splitting and concentration [7,8]. We refer to this diffractive optic as a "polychromat". Previously, we used the polychromat to increase the peak output power from two single-junction photovoltaic cells using 2-band spectrum splitting and concentration [8,9]. Here, we report the extension of this approach to 3 bands and a consequent increase in system power of 35.5%.

2. Working principle

The working principle of the polychromat can be understood from the configuration illustrated in Fig. 1(a). For simplicity, we utilize 1D polychromat, *i.e.*, the polychromat is pixelated along the X direction and uniform along the Y direction. There are 5001 pixels along the X direction and each pixel is 3 μm wide. The height of each pixel is an integer multiple of 23.81 nm, varying from 0 to a maximum height of 1.5 μm spanning 64 discrete height levels. The polychromat diffracts the incident light in such a way that low, medium and high energy spectral bands of light are concentrated on the left, center and right portions of the image plane, respectively. Each spectral band thus occupies one third of the space in the image plane, resulting in a concentration factor of 3X for each band. GaInP, GaAs and Si single junction solar cells were used to absorb these three different bands at the image plane. These solar cells were first chosen due to their availability and the polychromat was designed to accommodate them.

The dimensions of the GaInP and the GaAs cells are 5mm \times 5mm while that of the Si cell is 5mm \times 20mm. In order to ensure that all 3 cells were fully illuminated, the polychromat was designed to be 15mm \times 20mm. In addition, this polychromat unit cell was repeated three times along the X direction to account for the periodic boundary conditions used during

design [8,9]. As a result, the final device covers an area of 45mm × 20mm. The distance between the polychromat and the image plane was chosen to ensure that the shortest wavelength can be diffracted into the appropriate solar cell and this was set to 20cm. Note that this distance can be readily made smaller (to a few mm) when the pixel width is scaled to ~1μm or smaller [9]. The height distribution of the polychromat was determined by applying a modified version of the direct-binary-search algorithm to a rigorous optoelectronic model [9]. The optimization algorithm aims to maximize the power boost, defined as:

$$PowerBoost = \left(\sum_{i=1}^n P_{poly,i} - \sum_{i=1}^n P_{ref,i} \right) / \sum_{i=1}^n P_{ref,i} \quad (1)$$

In Eq. (1), n is the number of solar cells (or spectral bands), $P_{poly,i}$ and $P_{ref,i}$ are the peak output power densities of the i^{th} cell with and without the polychromat, respectively. The final pixel-height distribution is shown in Fig. 1(b). A magnified view of the left-most 100 μm of the polychromat shown in Fig. 1(c) reveals the multiple pixel heights.

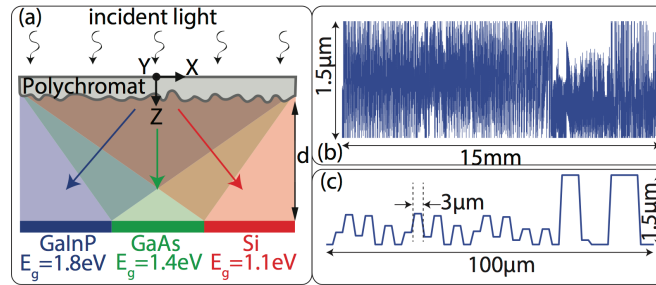


Fig. 1. (a) Schematic of the polychromat-solar cells configuration. (b) Height distribution of the designed polychromat. (c) Magnified view of the left-most 100 μm of the polychromat.

3. Fabrication of micro-optic

The polychromat was patterned in photoresist atop a glass substrate via grayscale laser lithography. The laser power at each pixel location was adjusted such that the appropriate pixel height is obtained after exposure and development. Details of this procedure and the associated calibration experiments are the same those described in ref [9]. An optical micrograph of the fabricated polychromat is shown in Fig. 2(a).

4. Optical characterization

We first measured the spatial-spectral point-spread function, *i.e.*, the intensity distribution along X in the image plane as a function of wavelength. The output of a supercontinuum source (NKT Photonics) was collimated and illuminated the polychromat at normal incidence. The fiber input to a spectrometer (Ocean Optics Jazz) was scanned along the X -axis in the image plane. We also simulated the spatial-spectral point-spread function using scalar diffraction theory [7,8] as shown in Fig. 2(b). The measured data plotted in Fig. 2(c) agrees very well with the simulation. We also calculated the optical efficiency as a function of wavelength, where the optical efficiency is defined as the ratio of power incident within the correct spectral band to the total incident power. The measured optical efficiency is shown as solid lines in Fig. 2(d) and agrees well with the simulated optical efficiency, shown as dashed lines. Discrepancies in these plots are attributed to fabrication errors as described later. Note that the colors represent the 3 spectral bands (see Fig. 1(a)).

Generally, better optical efficiency can potentially be achieved by shrinking the polychromat pixel width, increasing the maximum pixel height, augmenting the number of quantized pixel height levels, including more pixels in the polychromat design and increasing the gap between the polychromat and the solar cells [7]. Highly dispersive material can also increase the optical efficiency [9].

5. Electrical characterization

For electrical characterization, the 3 solar cells were placed at appropriate locations in the image plane one at a time. Current density and power density were measured for each device at different bias voltages with and without the polychromat. In order to normalize Fresnel reflections from the glass as well as residual light absorption within the photoresist, the reference measurements were taken with a glass substrate and unpatterned resist with the same thickness above the solar cells. Note that the beam was expanded to a diameter of $\sim 45\text{mm}$ before illuminating the polychromat, and the beam size was maintained the same for measurements both with and without the polychromat. The resulting plots are shown in Fig. 3. The blue and red curves correspond to the reference and the polychromat measurements, respectively. It is noted that the overall power densities are quite low due to the low illumination intensity, which was measured as $3.4\text{mW}/\text{cm}^2$. This was limited by the power output from our supercontinuum source. Nevertheless, all the solar cells demonstrate an improvement in performance with the polychromat. The short-circuit current-density (j_{sc}) of the GaInP, GaAs and Si cells are increased by 43.33%, 32.52% and 27.29%, respectively. This can be attributed primarily to the concentration. The open-circuit voltages (V_{oc}) are increased by 5.77%, 1.3% and 10%, respectively. As a result, the peak output power-densities are increased by 43.63%, 30.84% and 30.86%, respectively. The combined power-density from all 3 cells resulted in an increase of 35.52% when compared to the case without spectrum-splitting and concentration.

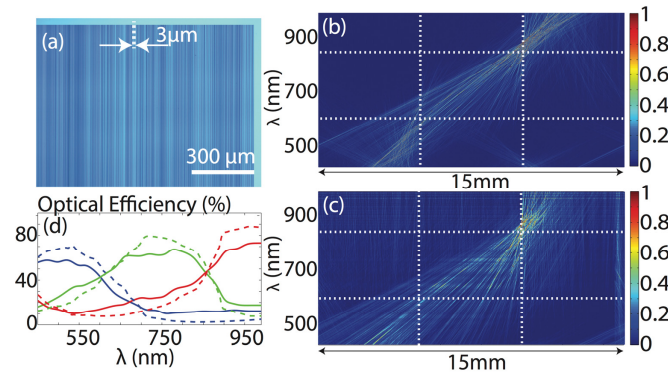


Fig. 2. (a) Optical micrograph of the fabricated polychromat. The spatial-spectral point-spread function of the polychromat: (b) simulated and (c) measured. White lines are shown to depict the boundaries of the 3 bands. (d) Optical efficiency as a function of wavelength: simulated (dashed lines), measured (solid lines).

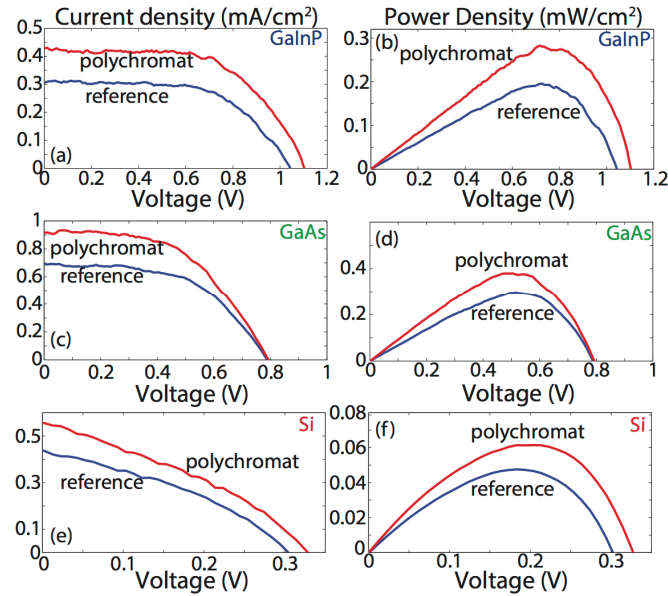


Fig. 3. Electrical characterization. Current density vs voltage for (a) GaInP (c) GaAs and (e) Si cells. Power density vs voltage for (b) GaInP (d) GaAs and (f) Si cells. Reference measurements are shown in blue, while spectrum-split measurements are in red.

These improvements can be explained with the help of the external quantum efficiency (EQE) plots of the 3 cells shown in Fig. 4(a). For the GaInP cell, any light of wavelength $> 700\text{nm}$ is not absorbed. Although wavelengths $< 700\text{nm}$ are absorbed within GaAs and Si, these photons produce current at a lower voltage than their intrinsic energy should allow. This is due to the thermalization loss. Therefore, by allocating those photons to the GaInP, one is able to minimize this loss. Similar arguments can be made for the GaAs cell as well. The overall effect is that the concentration of the appropriate spectral band by a factor of 3 results in an increase in the j_{sc} and a smaller increase in the v_{oc} . Minimization of the thermalization losses due to the appropriate spatial allocation of the photons also contributes to the increases in v_{oc} . Note that the best possible cells for spectrum-splitting exhibit non-overlapping EQE spectra. In such a case, where we can optimize the EQE by appropriate materials growth, the expected improvement can be quite large and can be comparable to the best multi-junction devices [10].

Note that the aforementioned improvement is based upon comparison to a reference of three solar cells of the same dimension without the polychromat. However, the total power density measured with the polychromat is lower than the case where the entire illumination aperture is filled with the best cell (GaAs here) without the polychromat. Our simulations confirm that this is primarily due to the poor performance of the specific Si solar cell that we used. It is clear from Fig. 3(e) that the j_{sc} of the Si cell falls far below those of GaInP and GaAs. In addition, the v_{oc} is also smaller than commercial cells under AM1.5 illumination partially because of the limited photon flux of our illumination. According to the J-V curve, the Si cell also suffers from reduced fill factor. On the other hand, if we assume ideal solar cells with the external quantum efficiencies shown in Fig. 4(a), our calculations indicate that this polychromat should enable an overall power density that is more than 3 times that produced by the best single-bandgap device of the same size as the polychromat aperture. Additionally, improving the optical efficiency (see Fig. 2(d)) by minimizing fabrication errors, discussed in the following section, is also able to increase the total power density output of the presented scheme.

6. Error analysis

Simulations predicted an increase of 61.79%, 70.55% and 39.79% in output power densities of GaInP, GaAs and Si solar cells respectively. The predicted increase in combined power density is 55.04%. The discrepancies between simulated and measured results are primarily due to fabrication errors. The pixel-height distribution of the fabricated polychromat does not perfectly match with the design heights primarily due to laser-intensity variations during the grayscale lithography and calibration processes. We illustrate this effect by plotting the designed and measured pixel-heights for a 160 μm -long segment of the polychromat in Fig. 4(b). By doing similar measurements over randomly selected two more segments, we estimated the pixel-height error to correspond to a standard deviation of 142nm.

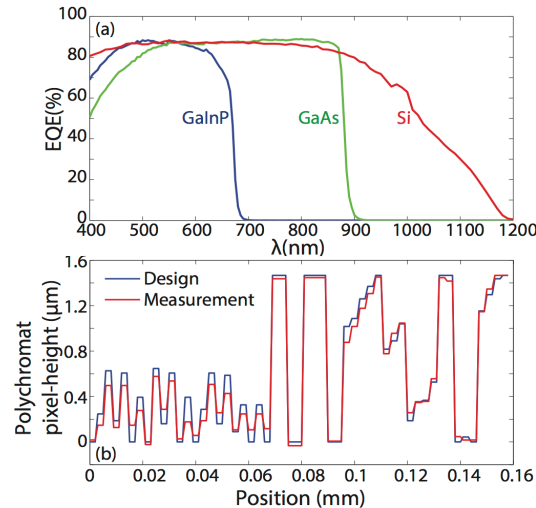


Fig. 4. (a) Quantum efficiencies of GaInP, GaAs and Si cells. (b) Designed (blue) and measured (red) pixel-height distribution along the x direction of the polychromat.

To gain insight into the effect of pixel-height errors on the device performance, we performed a statistical simulation. First, height errors were randomly selected from a normal distribution of zero mean and given standard deviation. Then, we applied our optoelectronic model to calculate the resulting increase in the output power-density, what we refer to as the power boost (see Eq. (1)). The power boost for each cell and the combined device (for all 3 cells) as a function of the standard deviation of the error distribution are shown in Fig. 5(a). It may be noted that for a standard deviation of 150nm (equivalent to the observed fabrication error), the combined power boost is $\sim 33\%$, close to the measured value of 35.5%. The corresponding impact on the optical efficiency is plotted in Fig. 5(b). The curves (dot-dashed lines) corresponding to the standard deviation of 150nm is comparable to the experimentally obtained curves in Fig. 2(d) (solid lines). From this analysis, we conclude that most of the discrepancy between the measured and the simulated power boost of 35.5% and 55%, respectively, is due to pixel-height errors during fabrication. Our current effort is focused on reducing this error via optimization of the fabrication process.

Defocus or variation in the distance between the polychromat and the image plane can also affect performance. To investigate this effect, we simulated the power boost and the optical efficiencies at defocus distances from -50mm to 50mm centered on the designed focus of 20cm . As shown in Fig. 5(c), for positive defocus, *i.e.*, as the image plane moves closer to the polychromat, the power boost of GaInP increases while that of Si decreases. This may be understood by appealing to the optical efficiency plots in Fig. 5(d). The optical efficiency plots exhibit red-shift and blue-shift due to positive and negative defocus, respectively. The red-shift allows GaInP to absorb more photons. Also, for negative defocus, the blue shift allows more high energy photons to reach the Si cell increasing its power boost

at the expense of the GaInP cell. The power boost of the GaAs cell decreases for both positive and negative defocus. As expected, the combined power boost is maximum at focus (zero defocus). Nevertheless, the depth-of-focus of this system defined as the defocus corresponding to a decrease in combined power boost of 20% is ~ 5 mm. Note that this is consistent with the low numerical aperture of the polychromat ($NA \sim 0.06$).

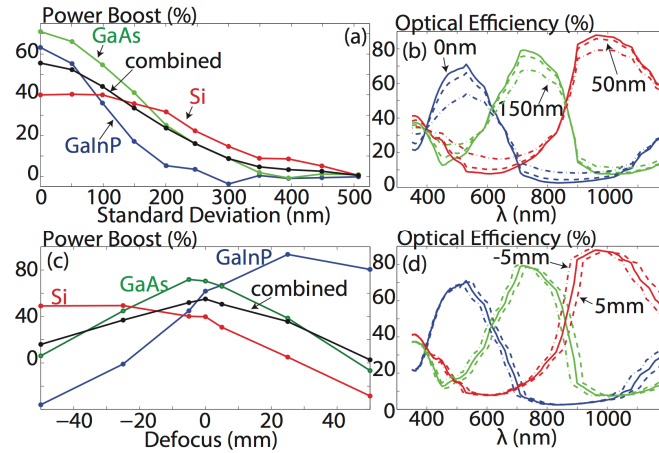


Fig. 5. Effect of errors. Variation (a) of power boost and (b) of optical efficiencies as a function of standard deviation of the polychromat height errors. Variation (c) of power boost and (d) of optical efficiencies as a function of defocus error.

7. Conclusion

Achieving high efficiency in a cost-effective manner is very challenging in photovoltaics. In this Letter, we describe progress towards this goal by utilizing a planar micro-optical element (polychromat) to spectrally split and concentrate sunlight onto 3 distinct solar cells, and measured an increase in output power of 35.5%. The polychromat can be inexpensively manufactured via high-volume stamping techniques [11,12]. The flexibility afforded by our approach can enable hybrid devices that combine multiple spectral bands and different concentration factors to achieve the best possible efficiency to cost ratios [9].

Acknowledgments

The project was funded by a DOE Sunshot Grant, EE0005959 and a NASA Early Stage Innovations Grant, NNX14AB13G. R.M. was partially funded by the Utah Science Technology and Research (USTAR) Initiative. We are grateful to Jose Dominguez-Caballero for assistance with the polychromat design, and Brian Baker, Steve Pritchett and Brian van Devener for support in the Utah Nanofabrication facility.